한국해양공학회지 제21권 제5호, pp 1-8, 2007년 10월 (ISSN 1225-0767)

On Long Wave Induced by a Sub-sea Landslide Using a 2D Numerical Wave Tank

WEON-CHEOL KOO* AND MOO-HYUN KIM*

*Ocean Engineering Program, Dept. of Civil Engineering, Texas A&M University, College Station, Texas, U.S.A.

KEY WORDS: Landslide, Tsunami, Boundary element, Run-up, Fully nonlinear, Numerical wave tank, Wave characteristics, Long wave

ABSTRACT: *A long wave induced by a Gaussian-shape submarine landslide is simulated by a 2D fully nonlinear numerical wave tank (NWT). The NWT is based on the boundary element method and the mixed Eulerian/Lagrangian approach. Using the NWT, physical characteristics of land-slide tsunami, including wave generation, propagation, particle kinematics, hydrodynamic pressure, run-up and depression, are simulated forthe early stage of long wave generation and propagation. Various sliding mass heights are applied to the developed model for a systematic sensitivity analysis. In particular, the fully nonlinear NWT results are compared with linear results (exact body-boundary conditionswith linear free-surface conditions) to identify the nonlinear effects in the respective cases.*

1. Introduction

A destructive Tsunami occurred at Papua New Guinea (PNG) in July 1998 due to submarine landslide, which produced unusually large run-up of 10m height. Landslide tsunami tends to be local, although possibly extreme, in its effect since the length-scale of a landslide is typically much smaller than that of an earthquake. The huge PNG waves swept three fishing villages of 3m land elevation. The case of PNG's landslide-generated tsunami is still of great scientific interest in that sub-sea landslide can generate such an unusually large run-up. It has been found that the earthquake occurred along the steep dipping reverse faults and the vicinity area of the event had a steep linear slope from coast. The PNG tsunami was thought to be generated by combining vertical displacement of ocean floor with the subsequent landslides on the steep slope.

The long wave induced by a submarine land-slide has two important characteristics; nonlinearity and frequency dispersion. The nonlinearity becomes even more important as the generated wave starts to deform and be amplified in shallow region. The frequency dispersion of the long wave mainly occurs when a sliding mass disturbs adjacent fluid causing free-surface depression.

The subsequent frequency dispersion can play an important role in determining both the offshore wave field and the shoreline flooding (Lynett and Liu, 2002). Depending on the shape and velocity of the sliding mass, the deformation of free-surface can change significantly.

The length of the generated wave is dependent on the size of effective landslide area in the fluid system. Larger effective area generates longer waves. Therefore, waves induced by an earthquake are usually longer than those by a landslide (Lynett and Liu, 2002).

Halmark (1973) first investigated the waves generated by a deformation of the bounding solid boundary in the fluid both theoretically and experimentally. He used a two-dimensional (2D) fluid domain with infinite lateral boundary and uniform depth. Recently, several researchers have studied the long wave generation induced by submarine landslide. Grilli and Watts (1999) developed a 2D boundary element model of an underwater landslide with 2^{nd}-order Taylor series expansion to simulate the early stage of free-surface deformation in time domain. Their works were extended to 3D numerical model (Grilli et al., 2002), 3D experiment (Watts and Grilli, 2003), and case studies (Watts et al., 2005). Lynett and Liu (2002) simulated submarine landslide-generated waves and run-up using a depth-integrated Boussinesq model and compared the results with a boundary integral equation method. Their results show that the Boussinesq model is less accurate in deeper water so that the model may not be applied to the case of wave propagation to the offshore.

Recently, the present authors developed a 2D fully nonlinear NWT based on boundary element method, mixed Eulerian and Lagrangian (MEL) approach and Runge-Kutta 4^{th}-order (RK4) time integration scheme, which is the most stable

교신저자 구원철: 735 International Blvd. #122, Houston, TX (U.S.A.) 1-425-770-5512 kwc1969@yahoo.com

nonlinear time marching method (Koo and Kim, 2004). Since the landslide-generated long waves possess strong and complicated nonlinearity, it is of great interest to compare the results of linear and fully-nonlinear free-surface conditions using the developed NWT to assess such nonlinear effects. It is also interesting to study the resulting wave propagation, flow kinematics, and induced pressure on seabed, and how they are influenced by the change of land-slide volume.

In this paper, using the developed NWT, various physical characteristics of the long waves induced by a Gaussian-shape submarine landslide with different heights are investigated, which includes a long wave generation, propagation, run-up and depression. In particular, water particle velocities above the submarine mass and hydrodynamic pressure on the sea slope are also studied. The fully nonlinear results are systematically compared with linear results to identify nonlinear effects in respective cases.

2. Mathematical Formulation

2.1 Boundary value problem and numerical schemes

The computational domain is assumed to be filled with homogenous, invicid, incompressible and irrotational fluid. Therefore, a fluid velocity in the domain can be described with the velocity potential. A space fixed rectangular coordinate system is used, where x is positive rightward from the left-end and z is positive upward from the calm water level. The sketch of the computational domain is illustrated in Fig. 1.

Laplace (continuity) equation can be applied as the governing equation in the entire fluid domain,

$$\nabla^2\phi = 0 \tag{1}$$

with the following boundary conditions:

1. Fully nonlinear dynamic and kinematic free surface conditions

$$\frac{\partial\phi}{\partial t} = -g\eta - \frac{1}{2}|\nabla\phi|^2 - \frac{P_a}{\rho}, \qquad \frac{\partial\eta}{\partial t} = -\nabla\phi\cdot\nabla\eta + \frac{\partial\phi}{\partial z} \tag{2}$$

where η, g and ρ are free surface elevation, gravitational acceleration, and water density, respectively. P_a represents air pressure on the free-surface assumed to be zero.

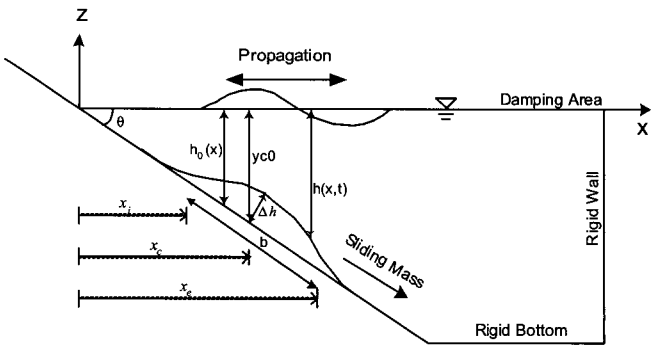

Fig. 1 Sketch of sub-sea landslide, $\theta = 6^0$, b=1m, $y_{c0} = 0.25m$ and Δh varies

2. Rigid boundaries on the sea-slope, bottom and vertical end-wall

$$\frac{\partial\phi}{\partial n} = 0 \tag{3}$$

3. Moving boundary condition for the submarine rigid slider on the sea-slope

$$\frac{\partial\phi}{\partial n} = \vec{V}_B \cdot \vec{n} \tag{4}$$

where $\vec{V}_B$ is a prescribed sliding body velocity and $\vec{n}$ is a unit normal vector on the body surface. Eq. (4) shows the fluid velocity adjacent to the moving body equals the body velocity in the normal direction.

Using the Green function (G) and the described boundary conditions above, the governing equation (Eq. (1)) over the domain can be transformed to the boundary integral equation given as

$$\alpha\phi_i = \iint_{\Omega}\left(G\frac{\partial\phi_j}{\partial n} - \phi_j\frac{\partial G}{\partial n}\right)ds \tag{5}$$

where, α is a solid angle (α = 0.5 or 1 when singularities are on the boundary or inside the fluid, respectively).

In order to solve Eq. (5), discretizing all boundary surfaces and placing a node on each segment/panel, which is called constant panel method (CPM) are used. So, the continuous integral equation could be modified as in the discrete form

$$\alpha\phi_i = \sum_{i=1}^{m}\sum_{j=1}^{m}\left[G_{ij}\frac{\partial\phi_j}{\partial n} - \phi_j\frac{\partial G_{ij}}{\partial n}\right]\Delta s_i \tag{6}$$

where G_{ij} is the matrix form of Green function corresponding to all boundary nodes, m is the total number of nodes on the entire boundaries and Δs_i is the length of each segment.

The Green function (G_{ij}) and its derivative ($\partial G_{ij}/\partial n$) are directly obtained from the instantaneous geometry of the boundaries in the fully nonlinear time domain. For 2D boundary problem, the simple source G_{ij} is given by

$$G_{ij}(x_i, z_i, x_j, z_j) = -(1/2\pi)\ln R_1 \tag{7}$$

where R_1 is the distance between source (x_i, z_i) and field points (x_j, z_j).

To solve the descretized boundary equation (Eq. (6)), the unknown boundary values should be separated from the known boundary values. The unknown values, in this case, are ϕs on moving body, rigid sea-slope, sea bottom, and right-end wall, and $\partial\phi/\partial n$ on free surface, while the known values are ϕ on free surface and $(\partial\phi/\partial n)$s on all other boundaries including prescribed sliding body boundary. Switching the known and unknown terms column by column, if necessary, the entire equation can be simplified as

$$\begin{bmatrix} \phi \\ \dfrac{\partial\phi}{\partial n} \end{bmatrix} = \bar{H}^{-1}\cdot\bar{G}\begin{bmatrix} \dfrac{\partial\phi}{\partial n} \\ \phi \end{bmatrix} \tag{8}$$

where the left bracket is unknown value of $[m \times 1]$ matrix corresponding to each node and the right bracket is boundary conditions on each boundary. $\bar{G}$ and $\bar{H}$ are the modified G_{ij} and $\partial G_{ij}/\partial n$ matrixes multiplied by element lengths (Δs_i). The $\bar{H}$ matrix includes $\alpha\phi_i$ term and $\bar{H}^{-1}$ is inverse form of $\bar{H}$.

The velocity potential (ϕ) and its normal derivative on each segment of the boundaries are obtained from solving Eq. (8). To obtain the time history of the velocity potential and the elevation (η) on the free surface, RK4 time-integration scheme as a time marching and the MEL method are used. These schemes are applied to Eq. (2) associated with Eq. (8).

Longuet Higgins and Cokelet (1976) first introduced MEL technique for the time simulation of nonlinear 2D waves. The MEL scheme has two-step procedure at each time step: (i) solving the Laplace equation in the Eulerian frame, and (ii) updating the moving boundary nodes and values in the Lagrangian manner. Applying a total derivative, $(\delta/\delta t) = (\partial/\partial t) + \vec{v}\cdot\nabla$, to Eq. (2) the fully nonlinear free-surface conditions in the Lagrangian frame can be modified as follows,

$$\frac{\delta\phi}{\delta t} = -g\eta - \frac{1}{2}|\nabla\phi|^2 + \nabla\phi\cdot\vec{v}, \quad \frac{\delta\eta}{\delta t} = \frac{\partial\phi}{\partial z} - (\nabla\phi - \vec{v})\cdot\nabla\eta \tag{9}$$

where $\vec{v}$ represents node velocity on the free surface.

To deal with the moving nodes on the free surface, material-node approach ($\vec{v} = \nabla\phi$), in which free-surface nodes trace water particles, is used. This approach makes the free-surface boundary-condition simpler but need to employ regriding process (rearranging the free-surface nodes every several time steps). The regriding prevents the nodes from crossing or piling up locally on the free-surface. In this study, the scheme is carried out at every time step to achieve better numerical stability.

A saw-tooth phenomenon on the free-surface causes the simulation to be unstable, which may be arisen by variable grid size against high-order aliasing. To avoid this numerical instability a Chebyshev 5-point smoothing scheme is used along the free surface during the time marching. This scheme has been proved in the authors' previous paper (Koo, 2003) and is applied at every 5 time-step in the present study.

An artificial damping zone is only located at the right-end of the domain to absorb the propagating wave energy. Both ϕ_n and η-type damping terms are added to the dynamic and kinematic free-surface conditions (Eqs. (10) and (11)). The optimized damping coefficients were adopted ($\mu_{01} = 1.5$ and $\mu_{02} = \mu_{01}$) after comprehensive test.

$$\frac{\delta\phi}{\delta t} = -g\eta - \frac{1}{2}|\nabla\phi|^2 + \nabla\phi\cdot\vec{v} + \mu_1\frac{\partial\phi}{\partial n} \tag{10}$$

$$\frac{\delta\eta}{\delta t} = \frac{\partial\phi}{\partial z} - (\nabla\phi - \vec{v})\cdot\nabla\eta + \mu_2\eta \tag{11}$$

where,

$$\mu_i = \begin{cases} \mu_{0i}\left[1 - \cos\left\{\dfrac{\pi}{2}\left(\dfrac{x-l}{l_d}\right)\right\}\right] & \text{for } x > l \\ 0 & \text{for } x \le l \end{cases}$$

l is the length of computational domain (no damping zone, 35xb for the present case) and l_d is the length of damping zone (7 x b for the present case) to be long enough to absorb all wave energy. The damping strength (μ_i) is designed to grow gradually to the target constant value to minimize wave reflection from the entrance of the damping zone.

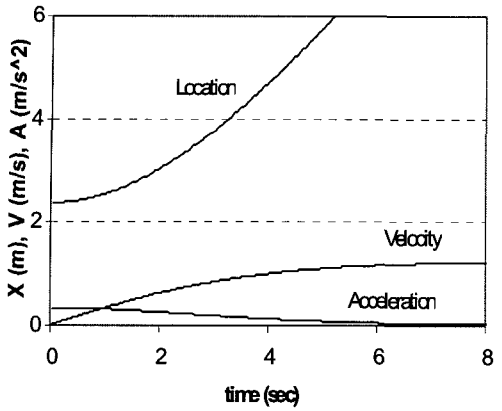

Fig. 2 Time history of slider location, velocity and acceleration, $\theta = 6^0$ and $y_{c0} = 0.25m$.

Details of numerical schemes described above are shown in authors' previous papers (Koo et al., 2004; Koo and Kim, 2004).

2.2 Sliding mass configuration

A Gaussian bell shape of sliding mass is similar to that employed by Lynett and Liu (2002) and the time-history of the landslide is described as

$$h(x,t) = h_0(x) - \frac{1}{4}dh \cdot \left[1 + \tanh\left(\frac{x - x_i(t)}{S}\right)\right]\left[1 - \tanh\left(\frac{x - x_e(t)}{S}\right)\right] \quad (12)$$

where, x_i and x_e are the tangent hyperbolic inflection points of the left and right sides of the mass, respectively, and S is a shape function enabling to control the steepness of the slide mass. Side boundaries and steepness factor are given by

$$x_i(t) = x_c(t) - \frac{1}{2}b\cos(\theta), \quad x_e(t) = x_c(t) + \frac{1}{2}b\cos(\theta), \quad S = \frac{0.5}{\cos(\theta)} \quad (13)$$

where, x_c is the horizontal center of the sliding mass. The angle of the slope is described by θ (degree). When the sliding vertical center, y_{c0} is known with a given slope, the initial horizontal center point, $x_{c0}(t=0)$ can be determined. The length between x_i and x_e along the slope is defined as b. The submarine slider moves as a solid body (non-deformable) and all the simulations presented in this study are non-breaking. The height of sliding mass at the center is given by

$$\Delta h = \frac{1}{4}dh \cdot \left[1 + \tanh(b\cos^2\theta)\right]^2 \quad (14)$$

The slider motion is determined by an approximate analytic solution (Watts, 1997; Grilli and Watts, 1999) and the velocity and acceleration at the slider center can be driven by the first and the second derivative of the displacement, respectively (see Fig. 2).

$$x_c(t) = x_{c0} + s_0 \ln\left(\cosh\frac{t}{t_0}\right) \quad (15)$$

$$\frac{dx_c(t)}{dt} = v_1 \tanh\frac{t}{t_0} \quad (16)$$

$$\frac{d^2x_c(t)}{dt^2} = a_0\left(\cosh\frac{t}{t_0}\right)^{-2} \quad (17)$$

where, $s_0 \equiv v_1^2/a_0$, $t_0 \equiv v_1/a_0$ are described by an initial acceleration (a_0) and terminal velocity (v_1), and these values are given by

$$a_0 = g\frac{\gamma - 1}{\gamma + C_m}\sin\theta, \qquad v_1 = \sqrt{gb}\sqrt{\frac{\pi(\gamma-1)}{2C_d}\sin\theta} \quad (18)$$

where, $C_m \approx 1.0$ and $C_d \approx 1.0$ are an approximate added mass and a drag coefficient of a circular cylinder, respectively. $\gamma = \rho_l/\rho_0$ represents a specific density of the mass. Watts (1997) pointed out that the slider motion with specific density $\gamma \approx 2$ is not sensitive to accurate values of added mass and drag coefficients.

2.3 Water particle velocity and wave pressure

Velocity potential (ϕ_i) at the target node inside the domain can be calculated directly from Eq. (6). ϕ_js and $(\partial\phi_j/\partial n)$s on the boundary at each time step are obtained as the time marching is carried out. The matrixes of G_{ij} and its normal derivative $\partial G_{ij}/\partial n$ are determined from the target node and instantaneous other boundary nodes.

After the velocity potentials (ϕ_is) at the target node and its neighbor points are obtained, their gradients ($\nabla\phi_i$, particle velocity) can be calculated using central difference formula. The pressure on the body can be calculated from the following Bernoulli's equation.

$$P = -\rho gz - \rho\frac{\partial\phi}{\partial t} - \frac{1}{2}\rho|\nabla\phi|^2 \quad (19)$$

Using the total derivative $(\delta/\delta t) = (\partial/\partial t) + \vec{v}\cdot\nabla$, Eq. (19)

yields

$$P = -\rho gz - \rho\frac{\delta\phi}{\delta t} - \frac{1}{2}\rho|\nabla\phi|^2 + \rho\nabla\phi\cdot\vec{v} \tag{20}$$

where, $\vec{v}$ is the node velocity on the sliding mass.

In case of a prescribed body motion, the total time derivative of velocity potential $\delta\phi/\delta t$ could be obtained directly from the high-order finite difference formula. When calculating the body pressure using Eq. (20), however, the node velocity ($\vec{v}$) is needed, which is not easy to be calculated. The node velocity was found to be significantly affecting the mean horizontal force even if the 1st-order forces can accurately be obtained. From this cause, the pressure can be obtained from Eq. (19) using the acceleration-potential method, which can directly calculate $\partial\phi/\partial t$ instead of $\delta\phi/\delta t$. The acceleration potential method, first formulated completely by Tanizawa (1995), is known to be the most accurate and consistent method to calculate the time derivative of velocity potential ($\partial\phi/\partial t$).

The following boundary integral equation for $\phi_t (= \partial\phi/\partial t)$ may be solved in the same manner as Eq. (5) with proper boundary conditions in the acceleration field.

$$\alpha\phi_{ti} = \iint_{\Omega}(G\frac{\partial\phi_{tj}}{\partial n} - \phi_{tj}\frac{\partial G}{\partial n})ds \tag{21}$$

The prescribed body boundary condition in the acceleration field is described as

$$\frac{\partial\phi_t}{\partial n} = a_x n_x + a_z n_z + \frac{\partial\phi}{\partial n}\left(\frac{\partial^2\phi}{\partial s^2}\right) \tag{22}$$

where a_x, a_z are body accelerations, n_x, n_z are normal vectors and s represents tangential direction on the surface, respectively. Since the first two acceleration terms of Eq. (22) affect the boundary condition appreciably, the third term is ignored in this study. Details of the acceleration potential method are shown in Koo and Kim (2004).

3. Results and Discussion

A long wave induced by a sub-sea rigid slider is simulated using the present fully nonlinear numerical wave tank (NWT). For various landslide mass heights, many important physical phenomena such as free-surface fluctuation, water particle velocities, hydrodynamic pressure on the slope, and wave run-up and depression on the beach are investigated.

To ensure the accuracy of the produced results, a series of convergence tests were carried out against the number of nodes and the size of time step. The node number (nodes/b) = 10.71 and the time step ($t/\sqrt{(g/b)}$) = 0.0313 are selected for the ensuing simulations.

3.1 Comparison with other methods

For the verification of the nonlinear NWT results, the present results are compared with those of linear NWT (Fig. 3) and depth-integrated Boussinesq method (Fig. 4). The linear result means that the free-surface condition is linearized but the body-boundary condition is satisfied at the instantaneous

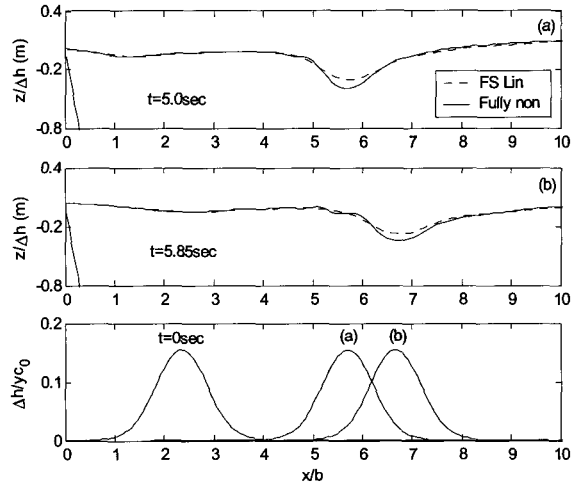

Fig. 3 Comparison of surface elevation, Δh = 0.0383; fully nonlinear simulation (= solid line), free-surface linear simulation (= dotted line).

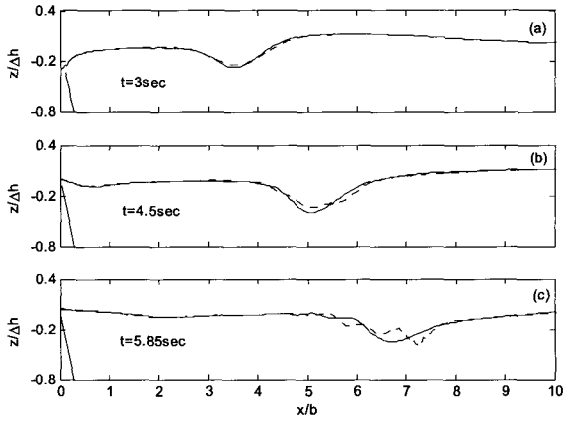

Fig. 4 Comparison of surface elevations of two different methods Δh = 0.0383; present (= solid line), depth integrated Boussinesq method (= dotted line)

position, so still nonlinear. It is seen that the free-surface depression is underestimated by the linear computation. As the submarine slider moves down, the location of free-surface depression follows the slider center.

In Fig. 4, the free surface snapshots of the present and Lynett and Liu's depth-integrated Boussinesq method are compared. The discrepancy between the two results increases as the slider moves down further. Since the Boussinesq equation is known to have accurate solutions only in shallow water, its accuracy is expected to be worse as the generated waves propagate toward the deeper water. It is also seen that the free-surface depression grows as the mass moves into deep water mainly due to the increasing slider velocity causing bigger pressure distribution.

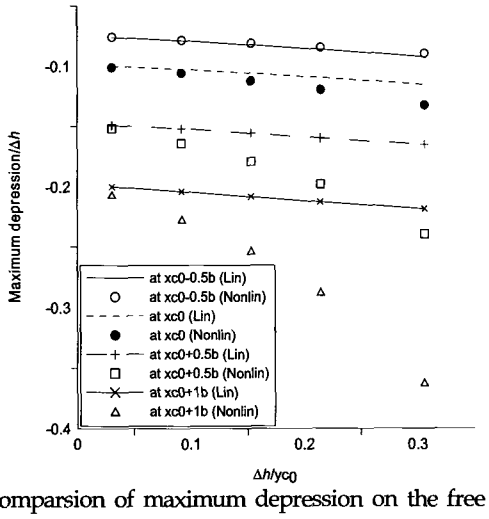

Fig. 5 Comparsion of maximum depression on the free surface with various Δh, Lin = linearized free surface condition, Nonliln = fully nonlinear free surface condition

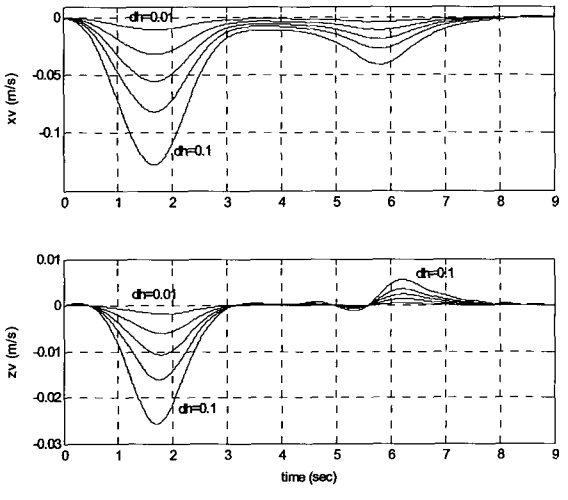

Fig. 6 Comparison of horizontal and vertical velocities at (x_{c0}, z/y_{c0} = 0.4)

3.2 Cases of various mass heights

In Fig. 5, linear and nonlinear amplitudes of the maximum free-surface depression for various land-slide heights (dh = 0.01, 0.03, 0.05, 0.07 and 0.1) are compared at four different locations near $x = x_{c0}$.

The difference between linear and nonlinear results increases significantly as the water depth and mass height increase. Since the linear calculation means the free surface boundary remains constant and the surface elevation is linearly proportional to the input, the rate of depression change is linear as the mass height increases. The depression change rate of nonlinear results, however, is quadratic because the free surface fluctuates significantly as the impact of slider on the surface increases. As explained in Fig. 3, since the linear calculation may underestimate the depression in the deep water region, the discrepancy between two results greatly increases as water depth increases.

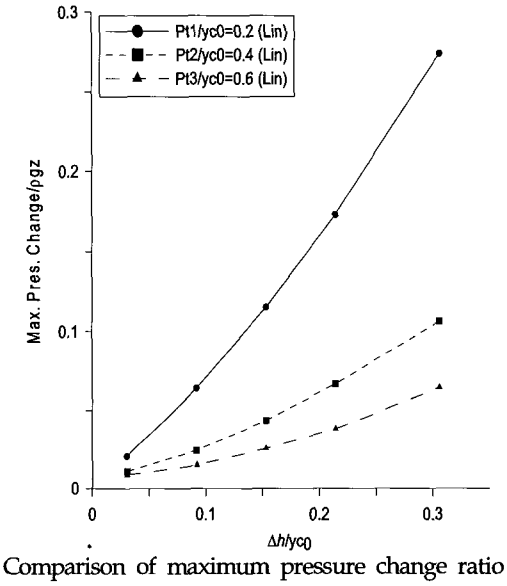

Fig. 7 Comparison of maximum pressure change ratio

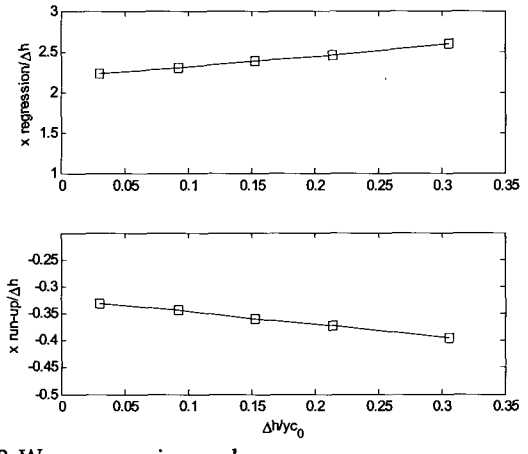

Fig. 8 Wave regression and run-up

Therefore, the nonlinear effect of the maximum depression could increase up to 65% compared with linear depression when $\Delta h/y_{c0}$= 0.3.

Time histories of water particle velocity at $x = x_{c0}$ and z/y_{c0} = 0.4 for various mass heights are shown in Fig. 6. Since the slider moves down in the positive x-direction on a 6-degree slope, the horizontal particle velocity is negative and about 5 times faster than the vertical velocity. The first pick of the water-particle velocity is induced by the initial motion of the landslide, while the second pick is due to the propagating waves generated by the slider.

The maximum pressure change normalized by hydrostatic pressure is plotted in Fig. 7. As expected, the dynamic-to-static ratio increases as the mass height increases. Since the surface fluctuation magnifies at the shallow water in case of long wave propagation, the effect of dynamic pressure significantly increases as the water depth decreases.

The change of wave regression and run-up against the mass height is shown in Fig. 8. Both magnitudes linearly increase with the mass height. It is found that the magnitude of regression is about 6-7 times bigger than that of wave run-up, which may be due to the direction of sliding-mass motion causing the adjacent fluid to push down to the sea bottom.

4. Conclusions

Using a 2D NWT based on boundary element method and MEL approach with fully-nonlinear free-surface conditions and a prescribed body motion, the time histories of free-surface depression and rising induced by a Gaussian bell shape sub-sea landslide are simulated in the time domain representing the early stage of the long wave generation and propagation. Various slider heights are applied to the developed model to investigate the sensitivity of results such as maximum depression, run-up, particle velocity, pressure on the slope. The present fully nonlinear model for submarine landslide is confirmed through comparison with published results by others. The nonlinear results are also compared with those with linear free-surface conditions to assess the respective nonlinear effects.

The magnitude of free surface depression increases as the mass height increases. The nonlinear effect of the maximum depression could increase up to 65% compared with linear depression when $\Delta h/y_{c0}$ = 0.3. This kind of nonlinear trend cannot be reproduced by linear computation. The time series of water particle velocity show two picks; the first pick is induced by the initial motion of the landslide, and the second pick is due to the propagating waves generated by the slider.

Since the surface fluctuation magnifies at the shallow water in case of long wave propagation, the effect of dynamic pressure significantly increases as the water depth decreases. The wave run-up and regression increase linearly as the mass height increases.

References

Grilli, S.T., Vogelmann, S. and Watts, P. (2002). "Development of a 3D numerical wave tank for modeling tsunami generation by underwater landslides", Engineering Analysis with Boundary Elements Vol 26, No 4, pp 301-313.

Grilli, S.T. and Watts, P. (1999). "Modeling of waves generated by a moving submerged body: Applications to underwater landslides", Engineering Analysis with Boundary Elements, Vol 23, pp 645-656.

Halmark, H.L., (1973). "A note on tsunamis: their generation and propagation in an ocean of uniform depth", J. of Fluid Mech., Vol 60, pp 769-799.

Koo, W.C. (2003). Fully nonlinear wave-body interactions by a 2D potential numerical wave tank, Ph.D. Thesis, Texas A&M University, College Station, TX, USA.

Koo, W.C. and Kim, M.H. (2004). "Freely floating-body simulation by a 2D fully nonlinear numerical wave tank", Ocean Engineering, Vol 31, pp 2011-2046.

Koo, W.C., Kim, M.H. and Tavassoli, A. (2004). "Fully nonlinear wave-body interactions with fully submerged dual cylinders", Int. J. of Offshore and Polar Eng., Vol 14, No 3, pp 210-217.

Longuet-Higgins, M. and Cokelet, E.D. (1976). "The deformation of steep surface waves on water: I. a numerical method of computation", Proc. of the Royal Society A, Vol 350, pp 1-26.

Lynett, P. and Liu, P.L.-P. (2002). "A numerical study of submarine-landslide-generated waves and run-up", Proc. of the Royal Society A", Vol 458, pp 2885-2910.

Tanizawa, K. (1995). "A nonlinear simulation method of 3-D body motions in waves (1st Report)", J. of Society of Naval Arch. in Japan, Vol 178, pp 179-191.

Watts, P. and Grilli, S.T. (2003). "Underwater landslide shape, motion, deformation, and tsunami generation", Proc. of the 13th Int. Offshore and Polar Eng. Conf., ISOPE 2003, Honolulu, HI, Vol 3, pp 364-371.

Watts, P., Grilli, S.T., Tappin, D.R. and Fryer, G.J. (2005). "Tsunami generation by submarine mass failure part II: Predictive equations and case studies", J. of Waterways, Ports, Coastal, and Ocean Eng., Vol 136, No 6, pp 298-310.

Watts, P. (1997). Water waves generated by underwater landslides, Ph.D. thesis, California Institute of Technology.

2007년 6월 30일 원고 접수
2007년 9월 4일 최종 수정본 채택